$M_{23}C_6$ Carbide Dissolution Mechanisms during Heat Treatment of ASTM F-75 Implant Alloys

H. MANCHA, E. CARRANZA, J.I. ESCALANTE, G. MENDOZA, M. MÉNDEZ, F. CEPEDA, and E. VALDÉS

The dissolution of $M_{23}C_6$ carbides in an ASTM F-75 alloy was experimentally followed, during a liquid-phase homogenization treatment, in as-cast and pretreated for partial carbide dissolution (PTPCD) specimens. The results revealed that before the fusion of the carbides, solid-state diffusion of the elements forming the carbides occurred. After the fusion of the carbides, a serrated interface developed. Treatment periods longer than 1000 seconds led to a liquid-carbide zone morphology showing the presence of dendrites within the liquid phase. Energy dispersion spectrometry (EDS) analysis revealed that the composition of such dendrites was very close to that of the α-phase matrix. The observed microstructure features are explained in terms of a solutal diffusion-driven mechanism leading to the growth of the matrix by consuming the liquid phase formed by the carbide fusion.

I. INTRODUCTION

IN surgical implant materials, a metal powder coating is commonly applied to enhance the implant fixation to bone and muscle by tissue ingrowth.[1–5] In cobalt-based alloys, such as ASTM F-75, the porous coating is formed through a sintering process at temperatures higher than those applied in conventional solution heat treatment (1300 °C *vs* 1220 °C).[2]

In addition, to improve wear[6] and mechanical properties, and prevent fatigue failure of implant cast alloys, different types of treatments are applied. Table I highlights the three main kinds of treatments that are applied to these materials, namely, conventional solution or homogenization treatments,[7–10] hot-isostatic pressing (hipping),[11,12] and carbide refining treatments.[13,14,15] Several authors[11,12] have reported that the best elongation values were obtained by hipping treatments and carbides refining by melt additions. Annealing generally produces undesired results, and conventional solution treatments require very close control of the treatment conditions. Regarding costs and technological level required by different kinds of treatments, the most expensive and higher demanding technology are hipping treatments, while conventional solution treatments have the lowest cost.

Due to intrinsic characteristics of the alloys, all of the aforementioned processes present technical difficulties that require a rigorous control of manufacturing processes in order to achieve the quality demanded on implants to be used in the human body. In conventional solution heat treatments, the temperature range available to dissolve most of carbides is very narrow. At low temperatures, spheroidization and coarsening of carbides are observed, but they are left out of the solution in the matrix of austenite.[16–19] Elevated temperatures cause carbide fusion, whereas low temperatures fall in a two-phase domain preventing complete homogenization and decreasing, considerably, the carbide dissolution kinetics.[9] Moreover, high-temperature conditions employed in the application of the metal powder coating causes incipient fusion of $M_{23}C_6$ carbides, producing materials of poor mechanical properties.

In this work, the $M_{23}C_6$ carbide dissolution of ASTM F-75 alloys was experimentally followed during a liquid-phase homogenization treatment, in as-cast and pretreated for partial carbide dissolution (PTPCD) specimens. The microstructural features observed are explained in terms of a solutal diffusion-driven mechanism leading to the growth of the matrix by consuming the liquid phase formed by the carbide fusion.

II. MATERIALS AND METHODS

Specimens from investment casting alloys conforming to ASTM F-75 specification with different carbon contents of 0.25 (AlloyLC) and 0.32 (AlloyHC) wt pct, hence different initial carbide fractions, were submitted to a liquid-phase homogenization heat treatment at 1250 °C, 1290 °C, and 1325 °C. As-cast and PTPCD specimens with dimensions of 10-mm length by 10-mm diameter, were immersed into a molten copper bath, previously stabilized at the treatment temperature, during periods of time of 1, 10, 100, 1000, and 10,000 seconds.

The PTPCD treatment, 1200 °C for 1 hour in a muffle-type furnace, was applied to the specimens with the lower carbon content. The chemical composition of the alloys is presented in Table II as determined by spark emission spectrometry (Lab S*). Carbon content was determined by the LECO* fusion technique. The microstructures of the as-cast and PTPCD samples were observed using optical and scanning electron microscopy. The carbide fraction was quantified by image analysis. The chemical composition of the liquid-carbide, the internal α-phase dendrites, and the

*Lab S is a trademark of Spectro Analytical Instruments GmbH, D-4190, Kleve, Germany.

*LECO is a trademark of LECO Corporation, St. Joseph, MI.

H. MANCHA, J.I. ESCALANTE, G. MENDOZA, and M. MÉNDEZ, Researchers, and E. CARRANZA, M.Sc., are with the Centro de Investigación y de Estudios Avanzados del IPN, 25000 Saltillo, Coah, Mexico. F. CEPEDAL and E. VALDÉS, Researchers, are with the Instituto Tecnológico de Saltillo, 25000 Saltillo, Coah, Mexico.

Manuscript submitted March 17, 2000.

Table I. Different Types of Treatments Applied to Co-Based Implant Alloys

Treatment Type	Treatment Sequence	Microstructure Response	Mechanical Properties			Reference
			YS (MPa)	UTS (MPa)	Elongation (Pct)	
Conventional treatment	cast + carbide dissolution	microporosity	557 to 482	740 to 689	3.11 to 11.3	7
	cast + TTS + aging	quasi-complete carbide dissolution	440 to 745	715 to 835	2 to 13.5	8
	cast + TTS	complete carbide dissolution	NA	NA	NA	9
	cast + TTS	partial carbide dissolution	520 to 590	630 to 858	14.5	10
Hipping	cast + HIP + TTS + aging	microporosity elimination	461 to 496	741 to 926	6.25 to 16	11
	cast + TTS + HIP	microporosity elimination	495	731	13	12
Carbide refining	(1.5 pct Nb + 1 pct Ta) addition	carbide refining, MC (TaC, NbC)	NA	NA	NA	13
	(Al, B, Cb, Ta, Ti, Zr) addition	carbonitride formation	498	1149	25	14
	(Cu, Ti, Nb, V, Zr, B) addition	NA	565 to 725	733 to 1010	8.2 to 14.6	15

Table II. Chemical Composition of the Alloys Used in This Work

Alloy	Elements (Wt Pct)							
	Cr	Mo	C	Si	Mn	Ni	Fe	Co
AlloyLC	27	5.3	0.25	0.51	0.7	0.42	1.4	bal
AlloyHC	27	5.5	0.32	0.48	0.75	0.38	1	bal

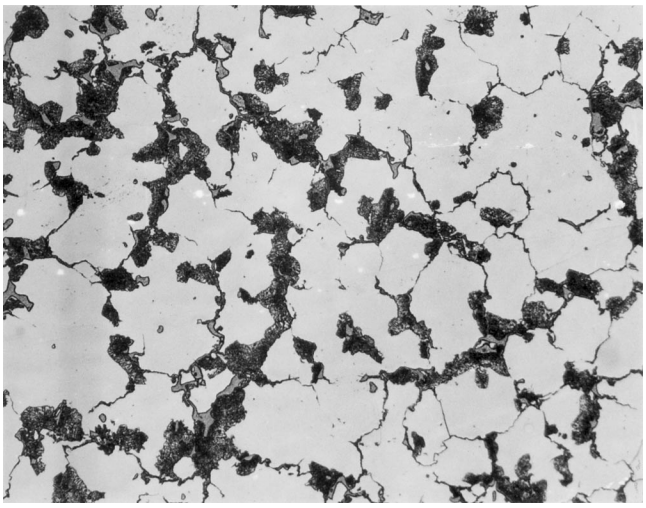

Fig. 1—As-cast microstructure of the ASTM F-75 implant alloys. Magnification 100 times.

matrix were determined using energy dispersion spectrometry (EDS).

III. RESULTS

The as-cast microstructure, presented in Figure 1, showed two types of $M_{23}C_6$ carbide morphology: blocky carbides, located in interdendritic regions; and lamellar structure carbides, mainly located at grain boundaries. Figure 2 presents micrographs showing the evolution of the microstructure during liquid-phase dissolution treatment of PTPCD samples treated at 1250 °C. Figure 2(b) reveals that the carbide fusion started after 10 seconds of treatment, and Figure 2(c) shows that the carbides were completely melted after 100 seconds. Before the fusion of the carbides, solid-state diffusion of the elements forming the carbides occurred, as shown in Figure 2(a). Following the fusion, a serrated interface developed, as observed in Figure 2(c). In the case of specimens treated for periods longer than 1000 seconds, the morphology of the liquid-carbide zone showed the presence of solid-phase internal regions. The EDS semiquantitative analysis, performed on a PTPCD specimen treated at 1325 °C for 1000 seconds, revealed that chemical composition of these solid regions, apparently dendrites, was close to that of the α matrix. Table III presents the average values of five point analyses performed on the matrix, dendrites, and the liquid region. It can be noted that the composition of the liquid region is different from those of the matrix and the dendrites. The dendrites have the same chemical nature as that of the matrix. Carbide fusion occurred earlier at 1290 °C and 1325 °C, as can be observed in Figure 3, which shows that carbides were already melted after 10 seconds at 1290 °C and 1 second at 1325 °C, whereas at 1250 °C, carbides were still solid (Figure 2(b)).

The change of carbide area fraction as a function of time, at the three treatment temperatures, is presented in Figure 4. It appears that the kinetics of carbide dissolution was similar regardless of the treatment temperature. However, from the shape of the curves, it seems there are at least two sequential stages in the change of the liquid fraction. The first stage, which lasts approximately 100 seconds, showed a fast decrease of the liquid-phase fraction, whereas in the second stage, the liquid fraction decreased at a slow rate.

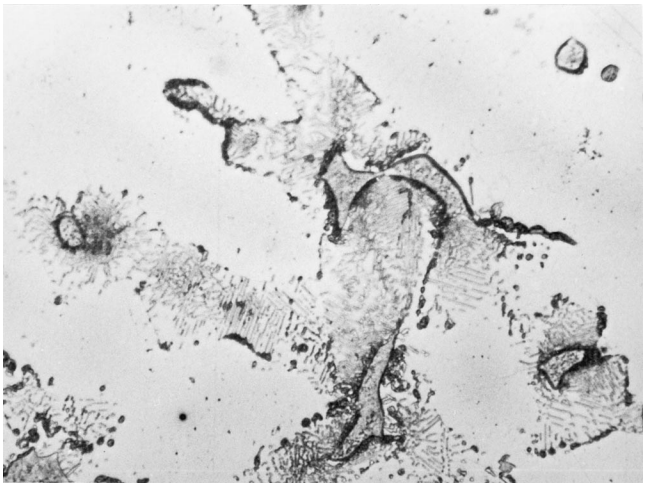

(*a*)

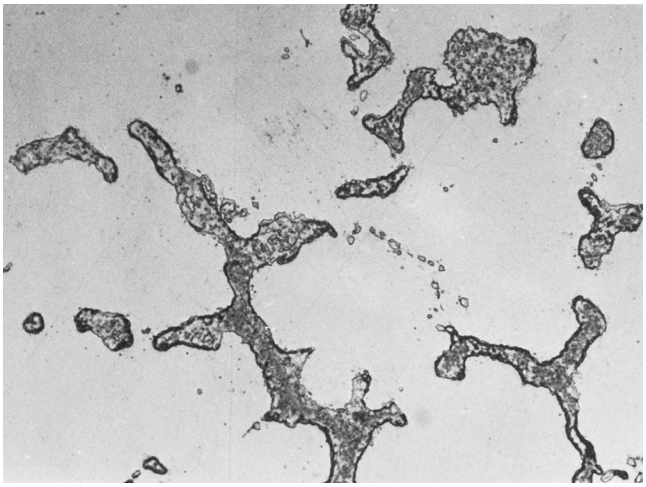

(*b*)

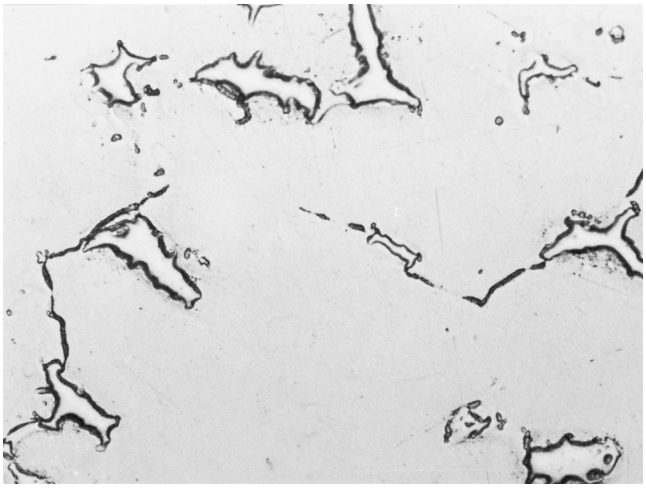

(*c*)

Fig. 2—Evolution of the microstructure during liquid-phase solution treatment of samples processed at 1250 °C, pretreated for partial dissolution of carbides: (*a*) magnification 500 times, 1 s; (*b*) magnification 500 times, 100 s; and (*c*) magnification 500 times, 10,000 s.

Table III. Results of Chemical Microanalysis of the Matrix, the Closed Internal Zones, and the Liquid Region (Bracketed Values Represent Standard Deviation)

	Element (Wt Pct)				
Zone	Co	Cr	Mo	Fe	Si
Dendrite	62.2 (0.5)	29.6 (0.3)	5.8 (0.6)	1.2 (0.3)	1.1 (0.1)
Carbide	44.6 (0.8)	38.3 (0.6)	15.0 (0.5)	0.9 (0.3)	1.1 (0.1)
Matrix	65.4 (0.3)	27.6 (0.4)	4.6 (0.3)	1.3 (0.5)	1.1 (0.6)

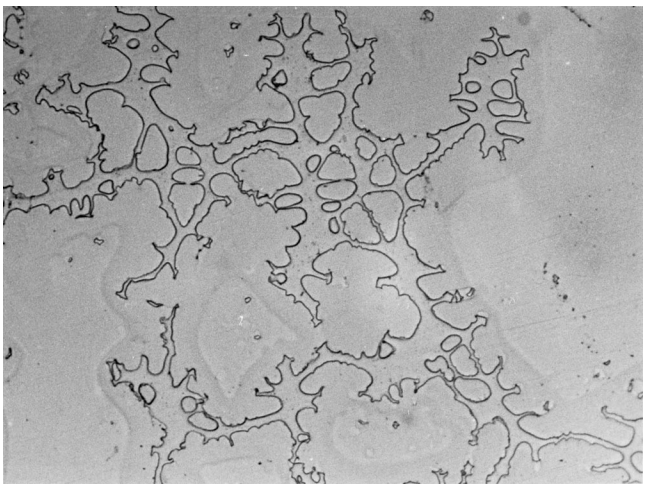

(*a*)

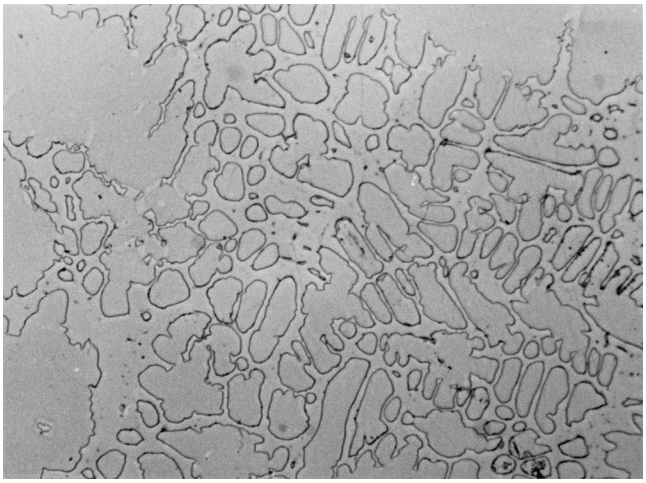

(*b*)

Fig. 3—Microstructures obtained at 1 s of treatment at (*a*) 1290 °C, magnification 500 times; and (*b*) 1325 °C, magnification 500 times, from the PTPCD specimens.

The microstructure evolution of as-cast samples was similar to that described above for the PTPCD specimens. However, in the as-cast specimens treated at 1325 °C, the initial stage of carbide dissolution occurred in a shorter period, as shown in Figure 5.

IV. DISCUSSION

A. *Driving Force for Microstructure Evolution*

The solidification microstructure of the ASTM F-75 alloys, which is formed by grains composed of interdendritic

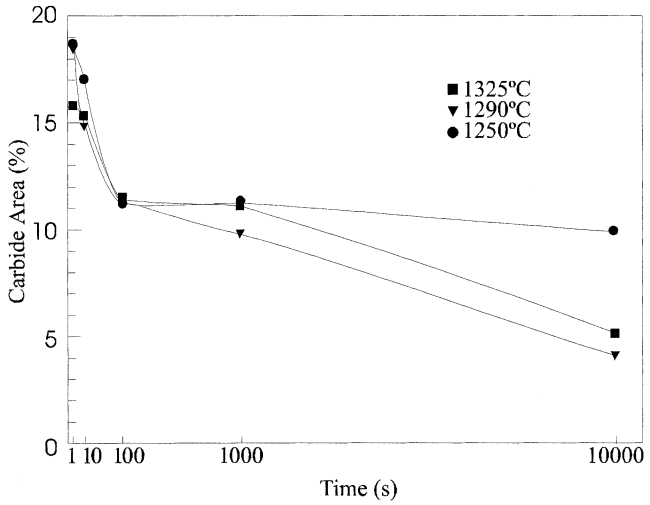

Fig. 4—Variations of the carbide fraction (area) with time for the PTPCD specimens at the three treatment temperatures.

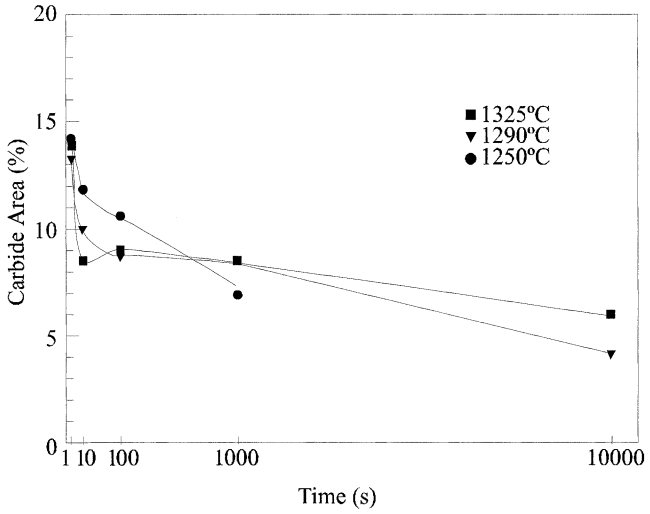

Fig. 5—Variations of the carbide fraction (area) with time for the as-cast specimens at the three treatment temperatures.

$M_{23}C_6$ carbides + α phase dendrites, has inherently a great compositional variation. Isothermal treatments at temperatures higher than the melting point of the $M_{23}C_6$ carbides tend to take the system to thermodynamic equilibrium. According to the second law of thermodynamics, the system tends to a more energetically homogeneous state, where the driving force would be the composition gradients. Diffusion of elements eliminates the composition gradients to achieve global chemical homogeneity. If the system reaches chemical equilibrium before the liquid is consumed by solid growth, a liquid fraction will remain. After elimination of concentration gradients, the system tends to homogeneously distribute the liquid throughout the solid α phase to attain thermodynamic equilibrium by entropy maximization. On the other hand, if the liquid is completely consumed before equilibrium is reached, the resulting system would comprise a single homogenous α phase. The results presented here show that during evolution of the microstructure the following three

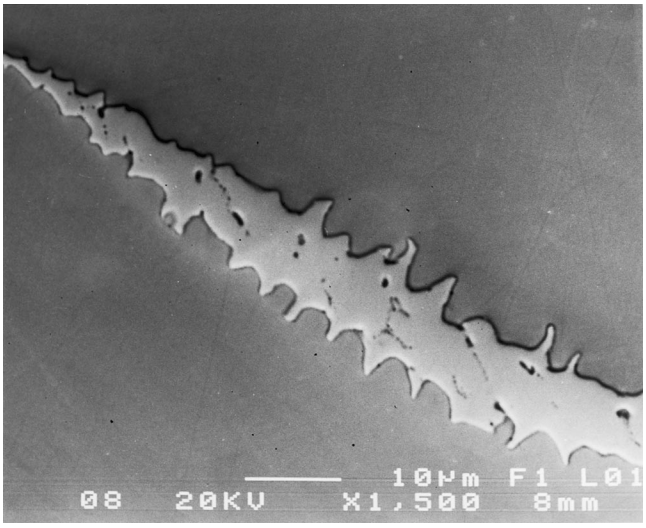

Fig. 6—Backscattered electron image showing the serrated interface.

phenomena occurred: a solid-state reaction of carbide dissolution before carbide fusion takes place, the melting of carbides with the development of a serrated boundary, and the growth of α-phase dendrites at the liquid expense.

B. *Carbide Dissolution by Solid-State Elements Diffusion*

In micrographs (a) and (b), presented in Figure 2, it is observed that during the first stage described for Figure 4, carbide decomposition took place through a solid-state reaction mechanism. In this figure, it is noted that the lamellar structure carbides dissolve more rapidly than the blocky carbides. This could be expected given that the α-phase/$M_{23}C_6$-carbide alternating lamellar structure of such particles allows a faster diffusion of the elements forming the carbides into the α phase. The carbide decomposition is considered to be associated with the thermodynamic instability of the carbides at the treatment temperatures, *i.e.*, the carbide forming elements have a greater chemical potential in the carbide than in the matrix.

C. *Melting of Carbides and Serrated Boundaries Development*

A solid-liquid interface with a low curvature is thermodynamically nonstable. Subsequent to the carbide fusion, this situation pushes the system toward a change in the interface curvature by developing a serrated shape. In this direction, once the carbides are melted, the solid-liquid interface moves, penetrating the liquid and producing the formation of a serrated interface, as shown in Figure 6. This, in turn, causes a decrease of the liquid fraction, an increase of the interface length, and a concurrent decrease in energy within the system. As a consequence, the interface takes positive and negative values of curvature.

D. *Growth of Solid α Phase*

The transfer of the elements constituting the liquid-carbide leads to different situations as a result of the serrated-shape

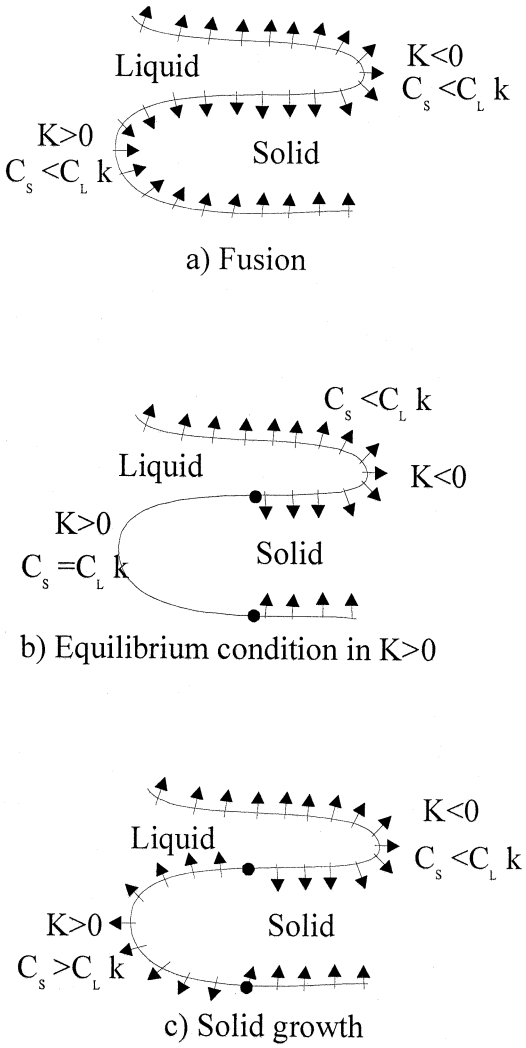

Fig. 7—(*a*) through (*c*) Schematic representation of the solute flux direction according to the interface curvature value.

of the interface. In the zones where the interface penetrates the solid, K takes values lower than zero. On the other hand, in the zones where the solid penetrated the liquid, the curvature of the solid-phase interface was positive ($K > 0$), which means that liquid surrounded the solid phase. This phenomenon is illustrated in Figure 7(a). In the $K > 0$ zones, because of the convex shape of the solid-liquid interface, the solute concentration in solid increases more rapidly than in the $K < 0$ zones. Thus, in the former zones ($K > 0$), the chemical equilibrium is attained and the transfer of solute stops, while in the latter zones, where $K < 0$, the transfer of solute to solid continues (Figure 7(b)). The solute transfer from liquid to solid continues with time and the content in the liquid phase reaches values lower than those of equilibrium, *i.e.*, $C_S > kC_L$. As this state is attained, the solute begins to be transferred back to the liquid at the $K > 0$ zones, as illustrated in Figure 7(c).

Under the conditions described in Figure 7(c), the elements that leave the solid phase create concentration gradients. Assuming thermal homogeneity in the specimen, the accumulation of solute ahead of the solid-liquid interface produces an undercooled liquid region, which favors the dendritic growth of the solid α phase in the liquid region.

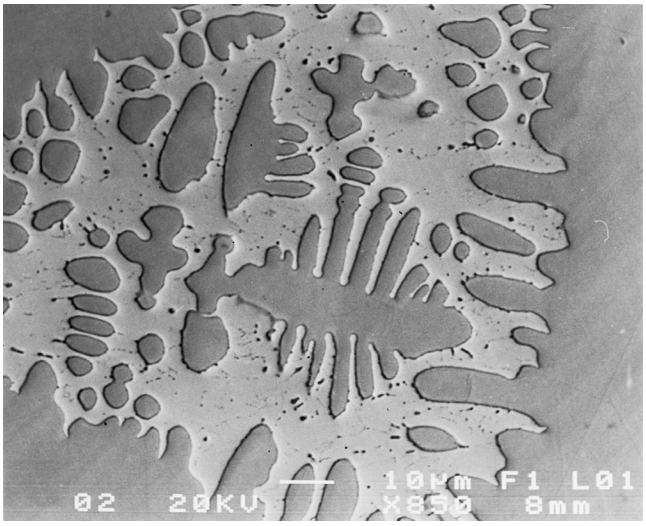

Fig. 8—Backscattered electron image of the α-phase dendritic structure observed inside the liquid region.

Hence, in order to attain chemical homogeneity, the diffusion process drives the growth of the solid α phase, leading to a complex morphology of the solid phase, as observed in Figure 2(c). The morphology of the two-phase zones, shown in Figure 2, became more complex with processing time as a result of the dendrite growth. Figure 8 presents a scanning electron micrograph showing the α phase dendritic microstructure observed inside the liquid region.

E. *Processing Temperature Effect*

From Figure 4, it can be remarked that during the first stage, the liquid-carbide dissolution rate in the PTPCD specimens was similar for all temperatures. Conversely, for specimens processed in the as-cast condition, the carbide fraction area at 10 seconds was very different for each temperature, increasing the fraction dissolved with temperature, as can be noted in Figure 5. However, from Figure 5, it seems that all the curves converged at 100 seconds of processing time when the solid-phase growth became the mechanism that predominantly controlled the rate of carbide dissolution, which decreased considerably beyond this point at all temperatures. The time consumed by the first stage for these specimens processed in the as-cast conditions was shorter than that required by the PTPCD specimens. This observation can be understood in terms of the compositional gradients, which were lower for the PTPCD specimens due to the previous treatment. As a consequence, the as-cast specimens had a greater driving force for solute diffusion. On the other hand, the time consumed by the first stage was only a small fraction of the total time required for the second stage. This indicates that increasing the temperature to accelerate the homogenization process does not bring any advantage.

The first stage observed in Figure 4, where the liquid-carbide fraction decreases rapidly, can be attributed to the diffusion process before chemical equilibrium is reached in regions with $K > 0$. The second stage can be attributed to a dendritic growth process occurring once the $C_S > kC_L$ condition is reached.

V. CONCLUSIONS

A study on the $M_{23}C_6$ carbide evolution during dissolution heat treatment of ASTM F-75 implant alloys was carried out at 1250 °C, 1290 °C, and 1325 °C on two types of specimens, namely, as-cast and PTPCD.

Two stages were observed during the carbide dissolution treatments at temperatures above the carbide melting point. The first stage, characterized by a rapid decrease of the liquid-carbide fraction, was attributed to the carbide decomposition through a solid-state diffusion mechanism of the carbide-forming elements and the development of a serrated interface. The second stage, which involved the growth of the dendrites in the matrix into the liquid phase, was considered a consequence of an undercooling developed ahead of the liquid-solid interface. The time needed to obtain a completely homogeneous microstructure was determined by the second stage, and the kinetic rate of the second stage did not appear to be affected by the temperature (1250 °C). This temperature seemed to be the most suitable from the technical and economical point of view.

ACKNOWLEDGMENTS

The authors wish to express their gratitude to CONACYT for financial support and their acknowledgment to M. Rivas, F. Vázquez and E. Córdova for technical support.

REFERENCES

1. T. Kilner, R.M. Pilliar, G.C. Weatherly, and C. Allibert: *J. Biomed. Mater. Res., Appl. Biomater.*, 1982, vol. 16, pp. 63-79.
2. R.M. Pilliar: *J. Biomed. Mater. Res., Appl. Biomater.*, 1987, vol. 21A, pp. 1-33.
3. B.S. Becker and J.D. Bolton: *Powder Metallurgy*, 1995, vol. 38, pp. 305-13.
4. B.S. Becker, J.D. Bolton, and M. Youseffi: *Powder Metall.*, 1995, vol. 38, pp. 201-08.
5. H.E. Placko, S.A. Brown, and J.H. Prayer: *J. Biomed. Mater. Res.*, 1998, vol. 39, pp. 292-99.
6. S.K. Yen, M.J. Guo, and H.Z. Zan: *Biomaterials*, 2001, vol 22, pp. 125-33.
7. K. Asgar and R. Peyton: *J. Dental Res.*, 1961, pp. 63-72.
8. D. Robertson: *J. Mater. Sci.*, 1983, pp. 391-401.
9. A.J.T. Clemow and B.L. Daniel: *J. Biomed. Mater. Res.*, 1979, vol. 13, pp. 265-79.
10. M.A. Gómez, H. Mancha, A. Salinas, J.L. Rodríguez, J. Escobedo, M. Castro, and M. Mendez: *J. Biomed. Mater. Res.*, 1997, vol. 34, pp. 157-63.
11. R. Hollander and J. Wulff: *J. Biomed. Mater. Res.*, 1975, vol. 9, pp. 266-69.
12. F.S. Georgette and J.A. Davison: *J. Biomed. Mater. Res.*, 1986, vol. 20, pp. 1229-48.
13. W.V. Youdelis and O. Kwon: *Met. Sci.*, 1983, vol. 17, pp. 379-94.
14. J. Cohen, R.M. Rose, and J. Wulff: *J. Biomed. Mater. Res.*, 1978, vol. 12, pp. 935-37.
15. L. Rademacher: U.S. Patent, No. 3,865,585, Feb. 1975.
16. D.V. Shtansky, K. Nakai, and Y. Ohmori: *Mater. Res. Adv. Techn.*, 1999, vol. 90, pp. 25-37.
17. C. García, G. Caruana, and L.F. Alvarez: *Mater. Sci. & Eng. A: Struct.*, 1998, pp. 211-15.
18. C. García, L.F. Alvarez, V. López, and J.A. Jiménez: *J. Mater. Sci.*, 1998, vol. 33, pp. 4096-4100.
19. M.R. Ghomashchi: *Acta Mater.*, 1998, vol. 46, pp. 5207-20.